Optimization of Fe-15Mn-5Si-9Cr-5Ni Shape Memory Alloy for Pipe and Shaft Couplings

Ana Velia Druker, Isidro Esquivel, Ariel Perotti & Jorge Malarria

Journal of Materials Engineering and Performance

ISSN 1059-9495
Volume 23
Number 7

J. of Materi Eng and Perform (2014)
23:2732-2737
DOI 10.1007/s11665-014-0981-0

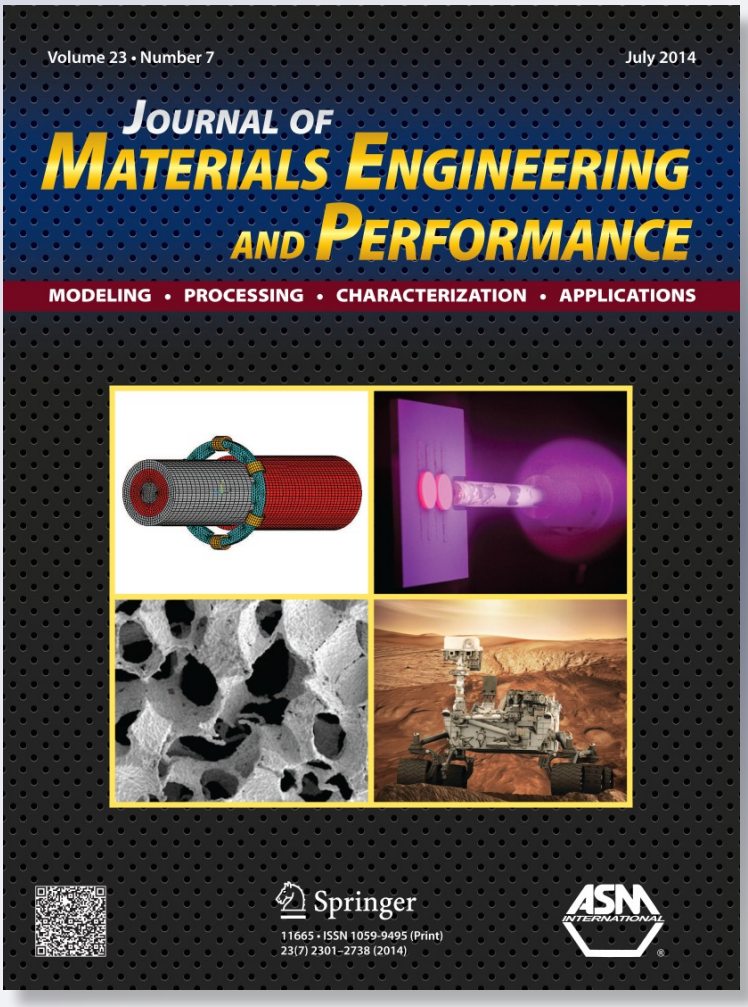

Springer

JMEPEG (2014) 23:2732–2737
DOI: 10.1007/s11665-014-0981-0

1059-9495/$19.00

Optimization of Fe-15Mn-5Si-9Cr-5Ni Shape Memory Alloy for Pipe and Shaft Couplings

Ana Velia Druker, Isidro Esquivel, Ariel Perotti, and Jorge Malarria

(Submitted September 23, 2013; in revised form December 20, 2013; published online April 12, 2014)

We investigated whether Fe-Mn-Si shape memory alloys could be manufactured into machine parts and devices, in particular pipe and shaft couplings. Accounting for the optimal parameters affecting shape memory properties, i.e., the chemical composition, the amount of processing deformation, the annealing temperature, and the correlation between the reversibility of the martensitic transformation and the conditions of the microstructure (particularly the role of crystal defects), we found that maximum recovery in a Fe-15Mn-5Si-9Cr-5Ni alloy is achieved by rolling at 800 °C followed by annealing at 650 °C. Furthermore, we investigated certain properties that establish technological feasibility limits to industrial production, including alloy weldability and mechanical response. Bending and tensile specimen tests determinate the expected behavior of parts joined by welding. We also developed an original process to produce the couplings. The degree of shape recovery of the couplings manufactured by this method depends on the annealing temperature after welding. The couplings annealed at 800 °C recovered 83% of a 3.6% permanent diametrical expansion.

Keywords advanced characterization, electron microscopy, superalloys

1. Introduction

The shape memory effect (SME) exhibited by certain metal alloys is due to a martensitic transformation that can be reversed by heating. High manganese Fe-Mn-Si alloys, which differ in various aspects to commercial steels, have this property. In this materials, the stable high temperature austenitic phase (FCC) transforms to ε martensite (HCP) near ambient temperature. Transmission electron microscopy (TEM) observations show that stacking faults which pre-exist in the austenitic matrix are sites for martensite plates nucleation. Very thin plates grow by the sliding of Shockley partial dislocations on alternating {111} austenitic planes (Ref 1). When the transformation is thermally induced, no macroscopic shape change is observed because martensite tends to self-accommodate producing plates in every possible sliding direction (Ref 2, 3). On the other hand, the transformation promoted by an applied stress only activates the most favorably oriented variant and the part shape changes (Ref 2). A SME occurs when the $\varepsilon \rightarrow \gamma$ reverse transformation takes place by inversion of the crystallographic path followed during the direct transformation. Recent research has shown that the defect structure can be controlled by thermo-mechanical treatments applied to the material (Ref 4). Particularly, the combination of rolling at intermediate temperature followed by annealing produces a nearly perfect SME in Fe-Mn-Si-based alloys (Ref 5, 6). When metals are rolled, dislocations multiply by mechanisms such as the Frank-Reed source. The energy stored hardens the material and subsequent annealing processes can enable recovery, recrystallization, and grain growth, depending on the time and temperature employed. Moreover, in alloys with low stacking fault energy (SFE) dislocations dissociate forming twins and stacking faults during the two stages of the thermo-mechanical process. Thus, the microstructural condition will depend on a combination of factors such as rolling temperature, reduction percentage, annealing time and temperature, and the alloy SFE (Ref 7). Most of these parameters also affect the mechanical and technological properties of the material. We have recently showed that rolling a Fe-15Mn-5Si-9Cr-5Ni (wt.%) alloy at 800 °C followed by annealing at 650 °C creates a structure that promotes the stress induced martensitic transformation instead of plastic deformation. After this process, the material recovers around 95% of a 3% permanent deformation making it suitable for practical applications like shaft and pipe couplings (Ref 8). However, the manufacturing background of seamless and welded (Ref 9– 13) couplings showed some difficulties and products made from this iron-based SM material have not yet been heavily marketed.

This work focuses on the characterization of the mechanical and technological properties of a Fe-15Mn-5Si-9Cr-5Ni (wt.%) alloy rolled at 800 °C and annealed at 650 °C, particularly the effects of welding on the mechanical and shape memory properties. We propose a new design for manufacturing couplings by forming and welding. Finally, we analyze the

This article is an invited paper selected from presentations at the International Conference on Shape Memory and Superelastic Technologies 2013, held May 20-24, 2013, in Prague, Czech Republic, and has been expanded from the original presentation.

Ana Velia Druker and **Jorge Malarria,** Facultad de Cs. Ex., Ingeniería y Agrim., Universidad Nacional de Rosario, Rosario, Argentina; and**,** Instituto de Física Rosario (CONICET-UNR), Rosario, Argentina. and **Isidro Esquivel** and **Ariel Perotti,** Facultad de Cs. Ex., Ingeniería y Agrim., Universidad Nacional de Rosario, Rosario, Argentina; Contact e-mail: malarria@ifir-conicet.gov.ar.

SM behavior of the coupling prototypes manufactured by this method.

2. Experimental Procedures

We prepared the alloy from commercial-quality raw materials by melting in an induction furnace under an argon atmosphere and casting into sand molds. After homogenizing at 1200 °C for 12 h, ingots were rolled at 1000 °C to 1.7 mm in thickness, and finished at 800 °C to obtain sheets 1 mm thick. Further annealing was performed at 650 °C for 30 min. Mechanical properties were evaluated by tensile tests in an Instron 3362 testing machine. To evaluate conformability, we used the simplest method for bending thin metal sheet which is to clamp a specimen and bending die in a vise, and then to bend the specimen over the die manually or with a nonmetallic mallet. Following the literature (Ref 14, 15), welding was done with the gas tungsten arc method; we used an ESAB Aristo Lud 450 welder, with a 2.4 mm diameter tungsten electrode held in a 10 mm diameter ceramic nozzle.

SM properties of welded samples were measured after bending 90° around a 40 mm diameter mandrel. Heating at 550 °C for 20 min (well above the A_f temperature) activated the reverse transformations. We photographed both the flat and bent samples before and after annealing, and measured the angles: θ_e, elastic recovery, and θ_r after annealing. The degree of bent shape recovery (DSR_b) was determined as follows:

$$DSR_b = \frac{90^\circ - \theta_r}{90^\circ - \theta_e} \cdot 100.$$

To evaluate the SM behavior of the couplings, we expanded them using an elastic sleeve and punch by applying a compressive load in the testing machine. We measured the diameter before and after the expansion (d_0 and d_1, respectively), and after annealing (d_2). The DSR of the couplings, DSR_C, was calculated as:

$$DSR_c = \frac{d_2 - d_1}{d_1 - d_0} \cdot 100.$$

XR diffractions measurements were performed with a Philips X-pert pro MPD goniometer using Cu $K\alpha_1/K\alpha_2$ radiation. To measure critical temperatures, we used the four-probe resistivity method. Microstructures were examined using an Olympus PME3 optical microscope (OM), a Phillips EM300 TEM operating at 100 kV (TEM), and a FEI Quanta 200 with field emission gun scanning electron microscope (SEM). Samples were mechanically and then electrolytically polished in a solution of 80% acetic + 20% perchloric acid to remove residual stresses. The foils were chemically thinned to 0.2 mm with a solution of 90% H_2O_2 + 5% HF + 5% HNO_3, and then electropolished with the double-jet technique in a 90% acetic + 10% perchloric acid solution at room temperature.

3. Results and Discussion

3.1 Chemical Composition and Critical Temperatures

Chemical composition is one of the most important factors for good SM properties since the critical transformation temperatures—M_s and A_s—and the SFE depend on it. To manufacture couplings it is desirable that the M_s is below room temperature and the A_s exceeds 50 °C, and the SFE should be as low as possible. Table 1 shows the results of chemical analysis and the values of the transformation temperatures of sheets rolled at 800 °C and annealed at 650 °C, measured by a resistivity method. Figure 1 shows this measurement in black along with another test corresponding to the same sheet after further heating at 800 °C for 5 min (orange curve). The last treatment will be tried when couplings are tested. The hysteresis cycle appears reduced, indicating that a short annealing at 800 °C reduced defects in the matrix and thus allowed interfaces to move more easily than in the sheet annealed at 650 °C. The 5 min exposure to 800 °C also caused the M_s and A_s temperatures increase to −82 and 123.5 °C, respectively, that indicated a sharper transition for the forward and reverse transformations.

3.2 Characterization of Mechanical Properties

Tensile tests provide information needed for the design of structures and mechanical components, such as yield strength, Youngs modulus, ultimate strength, and elongation. We prepared samples from the sheet processed by the thermo-mechanical treatment that produced material with the best SM properties. Curve (a)—black line—in Fig. 2 is representative of the mechanical behavior of the batch. The material deforms elastically up to a stress of 350 MPa; Youngs modulus, as

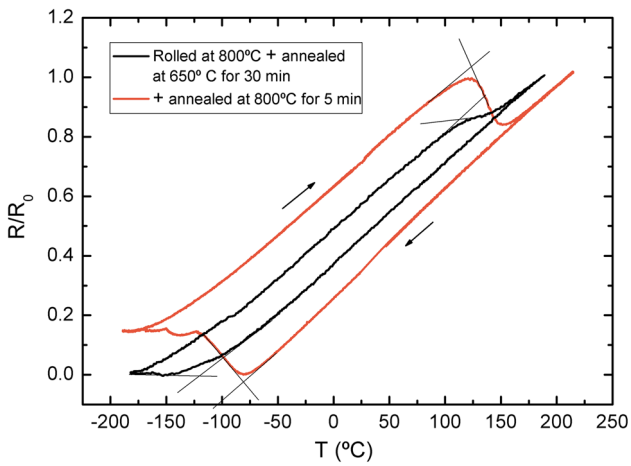

Fig. 1 Transformation temperatures of sheets treated in two different conditions

Table 1 Chemical composition (wt.%) and transformation temperatures (°C)

Fe, wt.%	C, wt.%	Mn, wt.%	Si, wt.%	Cr, wt.%	Ni, wt.%	M_s, °C	A_s, °C	A_f, °C
65.31	0.05	15.43	5.50	8.10	5.61	−121.5	113.1	159

calculated by the Instron Bluehill2 program, is 123.6 GPa. From this point permanent deformation may be due to $\gamma \rightarrow \varepsilon$ martensitic transformation and/or plastic slip. The hardening rate decreases continuously until an ultimate strength of 880 MPa is reached. The material fractures without necking after a total elongation of nearly 16%, as measured from the distance between two hardness indents.

3.3 Characterization of Technological Properties: Formability and Weldability

Among other important experiments, a simple bending test is useful to predict the formability of a material subjected to a single flexure stress during manufacturing. Thus we curved 1 mm thick samples 180° around a 40 mm diameter punch so that the deformation in the outer fiber was 2.5%. No damage, fracture, or surface irregularities appeared after these tests. The occurrence of the martensitic transformation during deformation was confirmed by heating the bent samples to 550 °C to activate the reverse transformation. The material recovered 157° of the original 180° deformation; this means 87% of shape recovery. This good SM behavior may be a problem during the couplings fabrication.

To evaluate the material's weldability and the influence of welding on the SME, we prepared samples of 1 and 2 mm thickness from sheets rolled at 800 °C. The TIG process parameters are given in Table 2.

After cutting by electrical discharge machining, samples belonging to the three batches were annealed at 650 °C. Visual inspection and macro-examination showed no defects in the face or root of the seams, and sectioning the weld beads revealed no internal defects and good weld penetration and fusion. During tensile tests, brittle fracture occurred in the weld beads after reaching a maximum stress of about 650 MPa, as can be seen in the corresponding σ-ε curve (b)—green line—in Fig. 2.

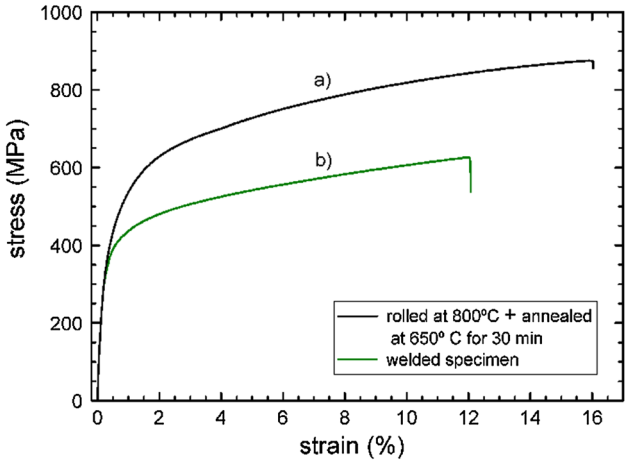

Fig. 2 Stress-strain curves obtained by tensile testing: (a) sample taken from a sheet rolled at 800 °C and annealed at 650 °C, (b) welded sample from the same sheet

OM observations of the welded sheet microstructure showed three zones: the welded zone (WZ), the heat-affected zone (HAZ), and the base metal (BM), as can be seen in Fig. 3. The NIC micrograph that can be seen in the inset was taken from an electropolished sample. The cellular-dendritic structure is due to solidification after welding. XR patterns of the BM (Fig. 4a) contain the characteristic peaks of austenite and low-intensity peaks (indicated by arrows in the XRD pattern) which we identify as the $Fe_5Ni_3Si_2$ precipitate. Both phases are recognizable in the high-magnification image shown in Fig. 5. The diamond-shaped marks are Vickers indentations showing an important hardness difference between the zones, $HV_{0.025}$ 967-1050 for the precipitate and $HV_{0.025}$ 302-325 for austenite. The quantity of second phase was estimated at $7 \pm 1\%$. TEM images presented in Fig. 6 show the precipitates, isolated dislocations, and a high density of stacking faults in the austenite. XR diffraction only detected austenite in the zones affected by the welding (Fig. 4b). Recrystallized grains in the HAZ have grown to about 300 μm, as the SEM image in Fig. 7 shows. Second phases almost disappeared from the material which would indicate that the temperature reached a range between 1000 and 1100 °C (Ref 16). Nevertheless some remnants of the previous structure—not-recrystallized- can be seen in the SEM image. The austenitic cellular-dendritic structure in the WZ contains a low-density distribution of defects, as can be seen in TEM images in Fig. 8.

The absence of dislocations in the austenitic matrix and the grain growth in the HAZ and the WZ degrade the SM properties. DSR_b of welded sheets was 87%, it is 8% lower than the 95% previously measured for the rolled sheets (Ref 8).

3.4 Process for Manufacture Coupling Prototypes

We designed a new device to manufacture coupling prototypes on the laboratory scale, which is manually operated in a hydraulic press. Figure 9 shows the assembly plane. The system, composed of upper and lower dies, a punch, and a bridge, was fabricated of medium-carbon steel (SAE 1045) quenched and tempered to HRc 48. As the manufacturing process must guarantee that the sheet only deforms plastically and no recoverable deformation is produced, threaded holes were added to accommodate stud bolts adjusted with wing nuts, Fig. 10. We deformed the sheet in successive stages in the lower die, bending it around the punch, which was horizontally supported by the bridge. Then, the bridge was replaced by the upper die, which closes the sheet into a ring. After this, we adjusted the wing nuts and the closed assembled set was heated in a furnace to 550 °C. When we heated the shape memory material above the reverse transformation temperature, the closed die/punch system avoided shape recovery. The stress developed within the fixture during annealing plastically

Table 2 Welding parameters

Sample thickness	Current, A	Voltage, V	Average power, kW	Slope up, s	Slope down, s	Pre-flow, s	Post-flow, s	Gas flow rates, ft^3/h
1 mm	28	12.3	0,36	1.6	1.6	2.2	3	18
2 mm (face)	42	12.7	0.52	1.6	1.6	2.2	3	18
2 mm (face and root)	28	14.2	0.4	1.6	1.6	2.2	3	18

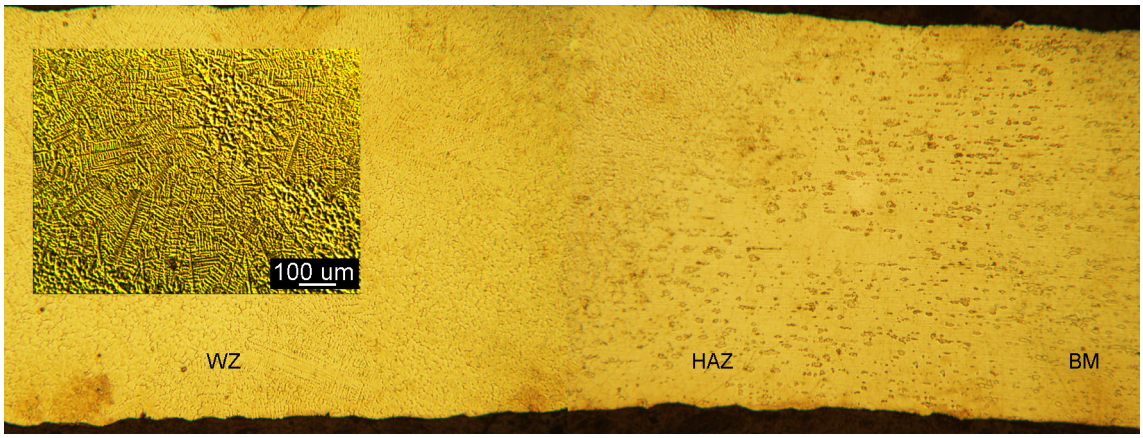

Fig. 3 OM image of the microstructure of the welded sheet: welded zone (WZ), heat-affected zone (HAZ), base metal (BM). The inset shows the cellular-dendritic structure in the WZ

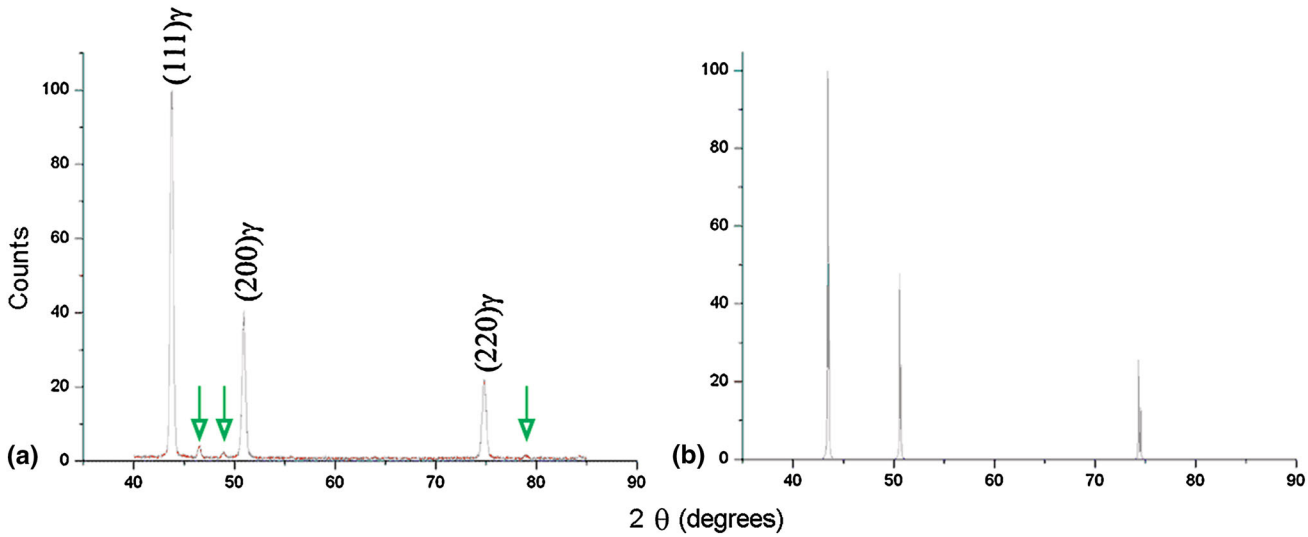

Fig. 4 XR patterns measured from (a) base metal, (b) heat-affected zones. Arrows indicate the characteristic peaks of the precipitates

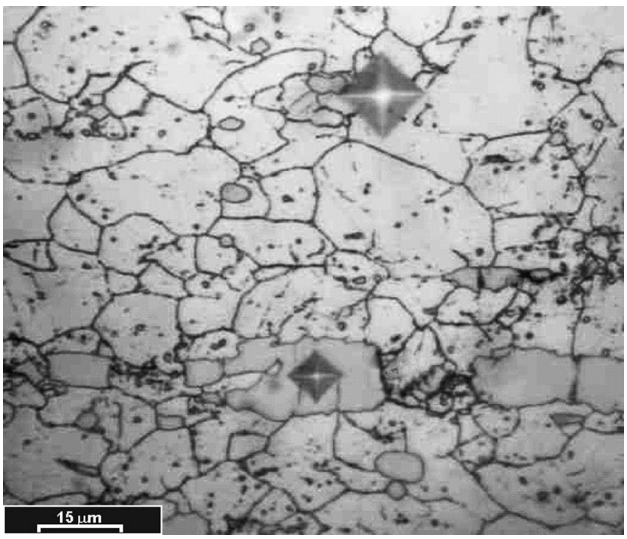

Fig. 5 Microstructure of the BM; indentations show the hardness difference between precipitates (bright grains) and austenite

deforms the austenite because the alloy is above the M_d temperature.

Welding was performed holding the conformed tube in order to prevent deformation during processing. The main welding conditions were direct current electrode negative of 28 A and argon flow rates of 8.4 L/min (18 CFH).

3.5 Degree of Shape Recovery of the Coupling Prototypes

The process to determine the SM behavior of the couplings begins expanding them circumferentially by using a set of an elastic sleeve and punch, as show the shop drawing in Fig. 11. After welding, we prepared three batches of samples, annealed at 650, 800, and 1000 °C respectively. Then we measured the outer diameter before expansion (d_0), during expansion (d_e), after elastic recovery (d_1), and after heating for shape recovery (d_2). The results show that the couplings annealed at 800 °C have very good shape memory behavior: they recovered 83% of 3.6% permanent deformation. On the other hand, annealing at 1000 °C degrades the properties and softens the austenitic matrix, leading to a DSR of only 48%. The DSR of couplings annealed at 650 °C was 79%, a value 5% lower than the

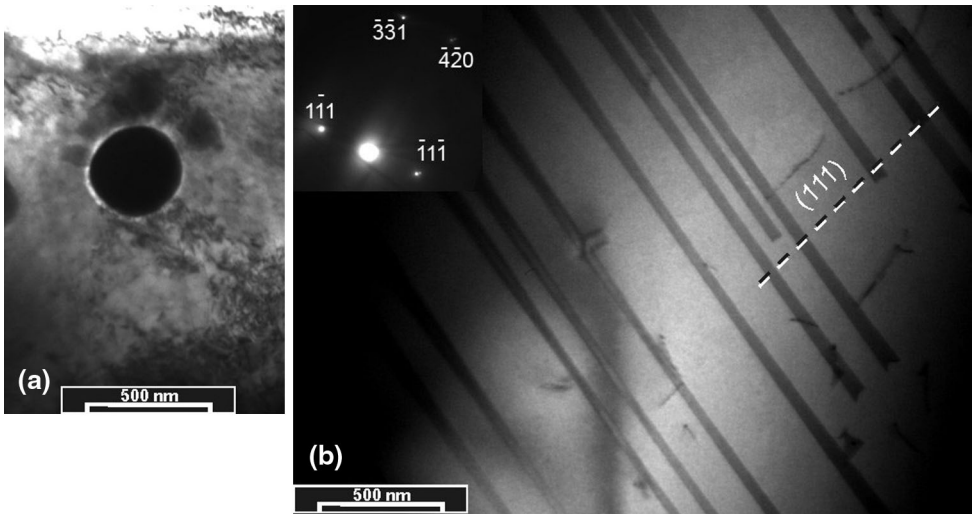

Fig. 6 TEM images from the BM showing a small quantity of precipitates, isolated dislocations and a high density of stacking faults in the austenite

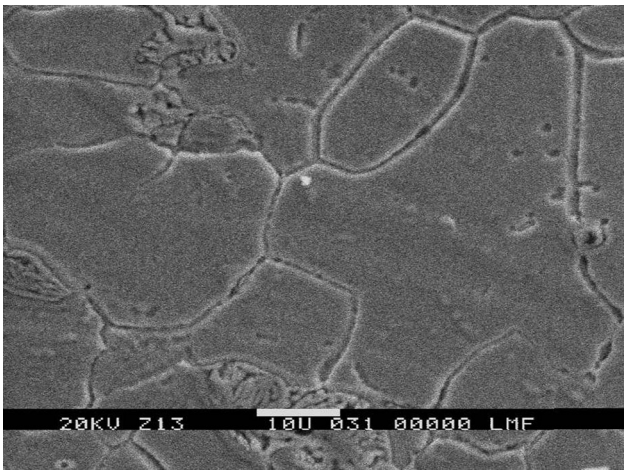

Fig. 7 SEM image from the HAZ showing that recrystallized grains have grown to about 300 μm

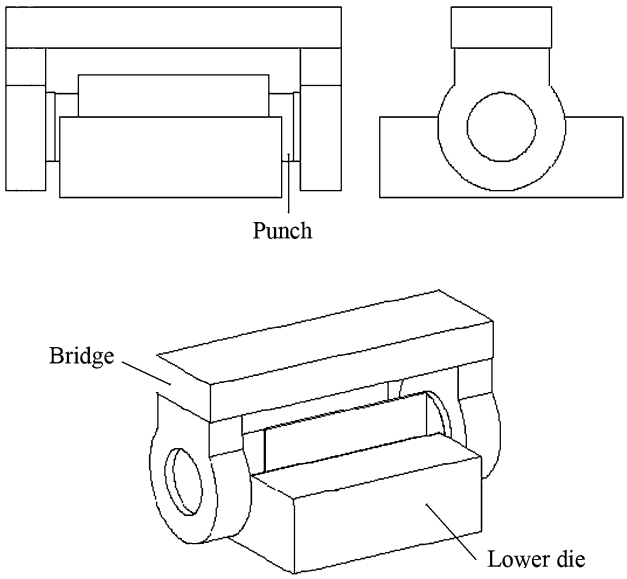

Fig. 9 Assembly plane of the device to manufacture coupling prototypes on the laboratory scale

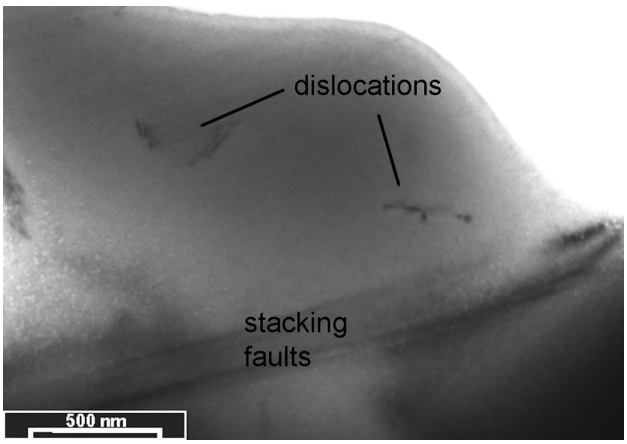

Fig. 8 TEM image from the WZ showing a low-density distribution of defects

Fig. 10 Photograph of the compound bending die

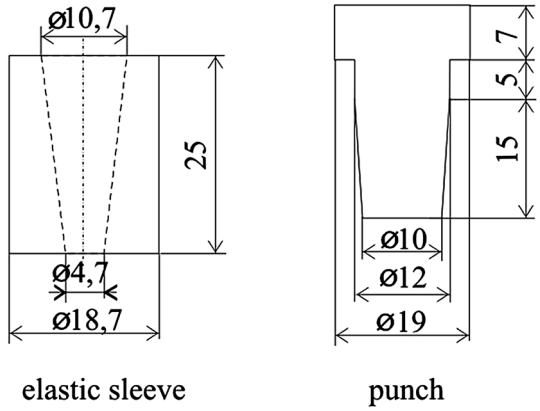

Fig. 11 Shop drawing of the elastic sleeve and the punch to expand the couplings

couplings annealed at 800 °C. This could be due to stresses accumulated in the material as a consequence of welding, which remain even after the heat treatment. SM properties achieved after annealing to 800 °C seem to be enough for many industrial applications.

4. Conclusions

The mechanical, technological, and recovery properties of shape memory ferrous welded couplings were analyzed and the main conclusions are:

(1) The Fe-15Mn-5Si-9Cr-5Ni alloy rolled at 800 °C and annealed at 650 °C have appropriate formability and weldability.
(2) Welding affects mechanical and shape memory properties. Samples fractured in the WZ and the DSR was reduced 9%, as measured with bend tests.
(3) An innovative method to manufacture couplings by forming and welding was presented, and we corroborated it to be successful.
(4) The DSR of the couplings manufactured by this method depends on the annealing temperature after welding. The couplings annealed at 800 °C recovered 83% of the 3.6% permanent diametrical expansion.

References

1. Z. Nishiyama, M.E. Fine, M. Meshii, and C.M. Wayman, *Martensitic Transformation*, Academic Press, New York, NY, 1978
2. A. Sato, E. Chishima, Y. Yamaji, and T. Mori, Orientation and Composition Dependencies of Shape Memory Effect in Fe-Mn-Si Alloys, *Acta Metall.*, 1984, **32**, p 539–547
3. T. Maki and K. Tsuzaki, *Proceedings of the International Conference on Martensitic Transformation (ICOMAT-92)*, C.M. Wayman and J. Perkins eds., Monterey Institute for Advanced Studies, 1992, p 1151
4. A. Druker, A. Baruj, and J. Malarría, Effect of Rolling Conditions on the Structure and Shape Memory Properties of Fe-Mn-Si Alloys, *Mater. Charact.*, 2010, **61**, p 603–612
5. N. Stanford and D. Dunne, Thermo-mechanical Processing and the Shape Memory Effect in an Fe-Mn-Si-Based Shape Memory Alloy, *Mater. Sci. Eng. A*, 2006, **422**, p 352–359
6. A. Baruj and H. Troiani, The Effect of Pre-rolling Fe-Mn-Si-Based Shape Memory Alloys: Mechanical Properties and Transmission Electron Microscopy Examination, *Mater. Sci. Eng. A*, 2008, **481**, p 574–577
7. J.C. Li, M. Zhao, and Q. Jiang, Alloy Design of Fe-Mn-Si-Cr-Ni Shape Memory Alloys Related to Stacking-Fault Energy, *Metall. Mater. Trans.*, 2000, **31A**, p 581–584
8. A. Druker, A. Perotti, A. Baruj, and J. Malarría, Heat Treatments of Fe-Mn-Si Based Alloys: Mechanical Properties and Related Shape Memory Phenomena, *J. ASTM Int.*, 2011, **8**(4), p 1–8
9. D. Dunne, *Shape Memory in Steels, in Phase Transformations in Steels*, Philadelphia, PA, Woodhead, 2012, p 83–125
10. T. Maruyama, T. Kurit, S. Kozaki, K. Andou, S. Farjami, and H. Kubo, Innovation in Producing Crane Rail Fishplate Using Fe-Mn-Si-Cr Based Shape Memory Alloy, *Mater. Sci. Technol. Ser.*, 2008, **24**, p 908–912
11. D.Z. Liu, D.F. Wang, W.Y. Ji, and W.X. Liu, *Proceedings of the 2nd International Conference on Shape Memory and Superelastic Technologies, SMST*, 1997, California, p 329-334
12. K. Hiroshi, H. Otsuka, S. Farjamic, and T. Maruyama, Characteristics of Fe-Mn-Si-Cr Shape Memory Alloys in Centrifugal Casting, *Scripta Mater.*, 2006, **55**, p 1059–1062
13. S. Kajiwara, A. Baruj, T. Kikuchi, and N. Shinya, Low-Cost High-Quality Fe-Based Shape Memory Alloys Suitable for Pipe Joints, Smart Structures and Materials, *Act. Mater. Behav. Mech.*, 2003, **5053**, p 250–261 (D. C. Lagoudas Editor, Proc. SPIE)
14. H.C. Lina, K.M. Lina, Y.C. Chuanga, and T.S. Chou, The Welding Characteristics of Fe-30Mn-6Si and Fe-30Mn-6Si-5Cr Shape Memory Alloys, *J. ASTM Int.*, 2000, **306**, p 186–192
15. Z.Z. Donga, T. Sawaguchi, S. Kajiwara, T. Kikuchi, S.H. Kimb, and G.C. Lee, Microstructure Change and Shape Memory Characteristics in Welded Fe-28Mn-6Si-5Cr-0.53Nb-0.06C alloy, *Mater. Sci. Eng. A*, 2006, **438-440**, p 800–803
16. B. Maji and M. Krishman, The Effect of Microstructure on the Shape Recovery of a Fe-Mn-Si-Cr-Ni Stainless Steel Shape Memory Alloy, *Scr. Mater.*, 2003, **48**, p 71–77